Dalton Transactions

Accepted Manuscript

ROYAL SOCIETY OF CHEMISTRY

www.rsc.org/dalton

Electrodeposition of Pluronic F127 assisted rod-like EMD/carbon arrays for efficient energy storage

[1,2]Avijit Biswal, [2,3]Bankim Ch. Tripathy, [1]Dan Li, [1]Manickam Minakshi*

[1]School of Engineering and Information Technology, Murdoch University, Murdoch, WA 6150, Australia

[2]CSIR, Institute of Minerals and Materials Technology, Bhubaneswar 751013, India

[3]Materials Engineering Department, University of British Columbia, Vancouver BC V6T 1Z4, Canada

Abstract

In the traditional Duracell battery, the results obtained to date remain marginal in terms of cyclability. The development of existing Zn-MnO_2 with superior electrochemical performance for use in alkaline rechargeable battery is reported. Electrolytic manganese dioxide (EMD) was synthesized from conventional manganese sulphate bath but having unique non-ionic surfactant (Pluronic F127) and activated carbon, in an electrolytic cell. The surface area and morphologies of as-prepared EMDs were influenced by the presence of these novel additives in the solution while the X-ray data revealed there was no noticeable change in the crystal orientations thus having all the EMDs structurally similar. The synergistic effect of the optimal ratio of surfactant to carbon powder produced rod-like arrays exhibiting larger surface area, which facilitates ion transport for better energy storage. It is interesting to note that EMD deposited in the presence of F127 showed better cycleability whereas in the presence of carbon, though showed better storage capability, was convoyed with poor efficiency when compared with the surfactant added, nevertheless, results are better than the existing Zn-MnO_2 technology (*additive free* EMD). Therefore, both the surfactant (50 mg dm^{-3}) and the activated carbon (5 g dm^{-3}) have been added together in the bath and the resultant EMD exhibits a high specific capacity and an excellent cycling stability. Moreover, the presence of surfactant and activated carbon improved the discharge capacity and its retention thus making this alkaline technology feasible to store renewable energy for future use. The synergistic effect and the mechanism involved have been discussed.

*E: minakshi@murdoch.edu.au

1. Introduction

Among the various energy storage devices, rechargeable batteries and electrochemical capacitors have drawn much attention in consumer electronic devices, electric vehicles and stationary applications [1-2]. The energy density of the battery devices is usually much high whereas the power density is quite high for capacitors. In the current scenario of energy crisis, continual attempts are underway to synthesize efficient energy materials from renewable and sustainable sources rather than the conventional fossil-fuels. Being an eco-friendly and cost effective material with long storage life, manganese dioxide (MnO_2) has been the choice as an efficient cathode material for the battery market since long [3-8]. Ever since 1866, when George Leclanche invented the galvanic cell, MnO_2 has been the principal constituent in dry cells. Today it is used in alkaline primary and secondary batteries. Electrolytic manganese dioxide (EMD) is preferred over natural and chemical manganese dioxides obtained from other sources due to its purity and better chemical reactivity [9-10]. EMD is one of the widely used cathode materials for alkaline batteries, lithium manganese primary batteries. It is interesting to note that Li-ion batteries, containing manganese derived from high purity EMD, are now in high demand for power vehicles, thus escalating the demand for EMD further [11]. EMD exhibits the greatest battery activity for most applications as quoted earlier. The zinc/manganese dioxide cell (Zn-MnO_2 commercially Duracell) in an alkaline potassium hydroxide electrolyte is a widely studied system. The reversibility of this cell as being a major bottleneck, most of the Zn-MnO_2 work has focused on incorporating metal oxides additives to manganese dioxide in order to make this cell rechargeable [12-19]. To the best of our knowledge, all the work has been oriented to physically adding these additives (ex-situ) to MnO_2. On the other hand, surfactant as an additive also plays an important role in enhancing the rechargeability of EMD by modifying the structure to a larger extent [20-28]. The reported surfactants in the literature [20-28] are quite well known to this field

and are pertained to cationic or anionic. In this work, the synthesis of EMD through an electrodeposition process with in-situ addition of non-ionic surfactant coupled with activated carbon in the electrolytic bath is reported here for the first time with an emphasis to enhance the cycling stability of alkaline Zn-MnO_2 battery.

It has been reported [29-36] earlier that non-ionic surfactant (Pluronic P123), amphiphilic triblock copolymers, act as structure-directing agents. The surfactant P123 has been used as a template and found to be very promising in the preparation of mesoporous silica and transition metal oxides with well-defined structures [29-36]. The chosen surfactant for this study named Pluronic F127 commonly known as F127 has been regarded as structure directing agent for synthesizing mesoporous MnO_2 [37], and also has been used as templates to synthesize mesoporous titania [38], MnO_2/C composite [39] or C/Si composite [40], as a precursor to synthesize mesoporous $LiFePO_4$/C composites [41] but has not been used towards MnO_2 electrodeposition. In the present work, F127 as a surfactant has been used in-situ during electrodeposition of manganese dioxide from sulphate solutions. The objective of the study was to evaluate its influence in terms of cycling behaviour of EMD.

Another objective of this work is to achieve a better conductivity through particle to particle contact between the MnO_2 for rapid faradaic reactions. It is quite well known in a battery field that MnO_2 being a semi conductive material, it shows high resistivity and the equivalent series resistance of MnO_2 is quite large (shown in the Electrochemical Impedance Spectroscopy section of this article) implying that a conductive material such as graphite, carbon black or activated carbon to be added ex-situ for increasing its conductivity and making it suitable for energy storage [15-16, 26-28, 42]. The use of graphene metal-oxide/hydroxide composite has also been reported for energy storage applications with promising results [43-45]. However,

research on in-situ addition of carbon or graphite to EMD during its electrochemical synthesis has not been widely researched. In the present work, an attempt has been made on potentiodynamic anodic co-deposition manganese dioxide/carbon composites by introducing activated carbon to the electrolytic bath. The objective is to have a uniform distribution of conductive carbon in the EMD matrix to achieve better conductivity. The EMDs synthesized from additive free bath or bath containing activated carbon (C) and/or surfactant (F127) were electrochemically evaluated by charge-discharge, cyclic voltammetry and electrochemical impedance analyses. X-ray diffraction analysis, thermal analysis, surface morphology and Brunauer, Emmett and Teller (BET) surface area analyses were also employed to evaluate the physicochemical properties of the material and those results are discussed along with electrochemical measurements.

2. Experimental

2.1. Material synthesis

Electrolytic manganese dioxide (EMD) was synthesized from a manganese sulfate in sulphuric acid bath containing 50 g dm^{-3} Mn and 25 g dm^{-3} H_2SO_4 at an anodic current density of 200 A m^{-2} in a thermostatic glass cell. The detail of the experimental set-up has been outlined in our previous work [26]. Pluronic F127 and/or activated carbon were added to the electrolytic bath at different concentrations and combinations. The hydrophilic non-ionic surfactant, Pluronic F127 is the BASF trade name of poloxamer 407, purchased from Sigma Aldrich belongs to the group of triblock copolymer consisting of a central hydrophobic block of polypropylene glycol edged by two hydrophilic blocks of polyethylene glycol (PEG) with molecular weight 12600 g. mol^{-1}. Activated carbon was purchased from Sigma Aldrich with a surface area of 1700 m^2/g.

EMDs synthesized in the presence of 0.5 and 5 g dm^{-3} of carbon were labelled as EMD+0.5C and EMD+5C respectively. EMDs synthesised in the presence of various concentrations of F127 were labelled as EMD, EMD+10F, EMD+25F, EMD+50F, EMD+100F, and EMD+500F for 0, 10 25, 50 and 100 and 500 mg dm^{-3} of F127 respectively. Similarly, the EMDs prepared in the presence of carbon *e.g.* 5 g dm^{-3} carbon and 50 mg dm^{-3} of F127 was labelled as EMD+5C+50F.

The anodic oxidation of Mn^{2+} to MnO_2 was carried out on a lead (Pb) anode placed in parallel to a stainless steel (SS) cathode. All experiments were carried out at 90±5°C for 4 h. Constant current was applied from a DC power supplier (MANSON, 0-30V, 2.5A). The dried mass of EMD after deposition was ground and sieved through a 53-μm mesh to obtain EMD powder. This was then washed repeatedly with deionized water until the sample was sulphate free. The EMD powder was finally dried and cooled in a desiccator followed by its physical and electrochemical characterizations. Morphological characterization was performed on EMD powders scraped from the anodes followed by thorough washing with deionized water.

2.2. Physical characterization

X-ray diffraction (XRD) patterns were measured with Siemens D500 X-ray diffractometer 5635 using Cu Kα radiation (l = 1.54 A^o) at 40 kV and 28 mA. The data were recorded from 10^o – 80^o with scan speed of 1° min^{-1}. Thermogravimetry analyses (TGA) of the samples were carried out by using a TA instruments (SDT 2960). Microstructures of the prepared samples were investigated by a high magnification Tescan Mira focussed ion beam-scanning electron microscope (FIB-SEM). Brunauer, Emmett and Tellet (BET) surface area measurement and porosity analysis were carried out by Micromeritics Tristar II Surface area and porosity analyser. For porosity measurements, the samples were degased at 100 °C overnight before analysis.

2.3. Electrochemical characterization

Galvanostatic charge-discharge measurements were carried out in a two electrode system by using a battery analyser (MTI Corp., USA operated by a battery testing system (BTS)). The electrochemical cell consisted of a cathode and an anode dipped in an aqueous electrolyte of potassium hydroxide (9M). The cathode consisted of an active material made of EMD (75wt %), carbon black (15wt %) and polyvinylidenefluoride (PVDF, 10 wt. %) mixed uniformly in an agate mortar in the presence of 0.3-0.4 mL of N-methyl-2-pyrrolidinone (NMP). The slurry was then coated on a graphite sheet of 1cm^2 and dried at 60 °C for an hour. Weight of the active material (EMD) was calculated from the weight of the graphite electrode before and after coating. A pure metallic zinc sheet was used as the anode. The supplied current density for these experiments was 2 mA cm^{-2} with discharge and charge cut-off voltages between 0.9 and 1.75 V respectively. Cyclic voltammetry (CV) and Electrochemical Impedance Spectroscopy (EIS) studies were carried out in a three electrode system using a BioLogic VSP-300 instrument. The working electrode used in this system was the active material coated graphite electrode, with metallic Zn sheet as the counter electrode. Mercury–mercuric oxide (Hg/HgO) served as the reference electrode with 9M KOH as the electrolyte. During CV studies the material was cycled in the potential window of 0.2 V to -0.6 V in cathodic direction with a scan rate of 0.2 mVs^{-1}. Impedance was recorded in the frequency range between 100 kHz and 1mHz with an amplitude of 5mV (vs Hg/HgO).

3. Results and discussion

Electrolysis

Electrodeposition of MnO_2 was carried out on lead anode at a current density of 200 Am^{-2} at 90 $^{\circ}$C for 4 h from an electrolytic bath containing manganese sulphate in an acidic medium (sulphuric acid) in the absence and presence of various combinations of activated carbon (C) and

surfactant (F127) tabulated in Table 1. It is showed that EMD when deposited from an additive free solution resulted in ~98% of current efficiency (CE) with energy consumption (EC) of 1.697 kWh kg^{-1}. Whereas, with the introduction of F127 (25 F) in the bath, the EC decreased to 1.501 kWh kg^{-1}. On further addition of F127 to a level of 100 and 500 F, showed slight increase in EC than the smaller level of 25 and 50 F, however all the EMDs deposited from a bath containing F127 showed lesser EC than the EMD obtained from a bath, free of F127. However, when activated carbon was added in excess of 5 g dm^{-3} in the bath, the CE decreased to 80% with slight increase in EC to 1.750 kWh kg^{-1}. On addition of both activated carbon and F127, the CE increased to 88% with little decrease in EC of 1.720 kWh kg^{-1}, suggesting the role of surfactant influenced in lowering the EC.

Physicochemical Characterization

The crystallinity of as-prepared MnO_2 produced from the sulphate bath in the absence and presence of activated carbon and/or the surfactant F127 is clearly revealed from the powder XRD patterns shown in Figure 1. All the samples are comprised of five major peaks at various 2θ values such as 22^o (110), 37.2^o (021), 42^o (121), 56^o (240/221) and 68^o (002/061). The diffraction peaks can be indexed to an orthorhombic phase of γ-MnO_2 with lattice constants: a = 8.70 Å, b = 2.90 Å and c = 4.41 Å. These cell parameters are in good agreement with the standard values of JCPDS card no. 65–1298 (a = 9.27 Å, b = 2.87 Å, c = 4.53 Å). The crystal structure of the EMDs was identical and seems to be independent of the concentrations of carbon and/or F127. These results confirm that irrespective of the additive concentrations and their nature, all the electrodeposited EMD samples are structurally identical.

Thermogravimetry (TG) analysis was carried out to determine the effect of C and F127 on the thermal stability of the EMD samples. As shown in Figure 2, all the samples showed weight loss due to physisorbed and chemisorbed water within the range of 110-270 $^{\circ}$C respectively. The

weight loss corresponding to the formation of Mn_2O_3 and Mn_3O_4 were observed after 500 and 950 $^{\circ}$C respectively. It can be noted that, the EMD deposited in the presence of C (EMD+5C) showed no weight loss after 600 $^{\circ}$C, suggesting higher thermal stability of EMD in the presence of carbon. EMD deposited from a bath containing both C and F127 also had similar response to thermal treatment confirming the thermal stability of samples.

Figure 3 showed the nitrogen adsorption-desorption isotherms and the corresponding Barrett–Joyner–Halenda (BJH) pore-size distribution curves (inset). The surface areas of as-prepared EMD, EMD+50F, EMD+100F, EMD+500F, EMD+5C and EMD+0.5C were 89.77, 119.60, 126.04, 115.15, 119.80, and 107.46 m^2g^{-1}respectively. This clearly indicates that presence of F127 as well as carbon might have played significant role in modifying the morphology and hence surface area of EMDs. From the nitrogen adsorption isotherm it was clearly observed that EMD showed slightly different behaviour during adsorption. The amount of absorption gradually increased as the pressure lowers and its tendency of adsorption also slowed down in the relative pressure range of 0.5 to 0.8. However, EMDs in the presence of F127 and C have the tendency of increasing adsorption at lower relative pressure. The adsorption and desorption behaviour corresponds to the type IV isotherm with a H2 type hysteresis loop characteristics of mesoporous materials, with loop shifting to a higher relative pressure approaching P/P_0 = 0.98 suggesting large number of mesopores. No significant difference was observed from the BJH pore size distribution curve; however EMD samples modified with F127 or C showed lower pore volume than the EMD produced in their absence. The lower pore volume of the modified EMD could help in shortening the path for easy transport of ions in the matrix and improving the rate performance of the battery material.

Surface morphologies of the as-prepared EMD samples exhibits mesoporous characteristics as identified by field emission SEM images shown in Figures 4a – d and 5a – b. As observed from the images (Figs. 4 – 5) on introducing F127 reduces the size of the crystallites and presence of carbon in the bath increases the size of the crystallites with different orientation. The sample EMD+50F (in Fig. 4b) showed interconnecting nanoscale pore channels giving sufficient evidence about the porous nature of the material. On increasing the F127 concentration in the bath to 100 mg dm^{-3} the modified material showed a more compact morphology, comprised of needle like grains, however, needles get agglomerated and oriented differently on increasing the concentration to 500 mg dm^{-3}. This represents that the non-ionic surfactant (F127) plays a role of structure directing agent during the electrodeposition of MnO_2. The obtained morphology again differs in terms of in-situ addition of carbon in the bath and those images are shown in Fig. 5. EMD obtained from a bath containing C showed larger crystallites (Fig. 5a) however each large crystallite seems to be an agglomerate form of smaller crystallites within the range of 10-20 nm. EMD deposited from a bath containing both C and F127 showed (in Fig. 5b) quite intermediate (controlled) behaviour of the two different additives. The sample EMD+5C+50F showed needle/rod-like shaped crystallites initiating from the influence of C whereas a networking structure may be from F127. This could provide effective pathways for ion transport. It is interesting to note that in all the cases the crystallites were showing nano characteristics and were of spindle (rod-like) shapes (over all view) having length within 50-100 nm range and width in the range of 10-20 nm. The obtained pore size distributions are in agreement with Peng's work [39].

Electrochemical characterization: Energy Storage

Galvanostatic (charge-discharge)

The performance of the as-prepared EMDs synthesized in the absence and presence of F127 and/or C was evaluated by charge-discharge, cyclic voltammetry and impedance studies. During galvanostatic charge-discharge study, the EMD electrodes (prepared as discussed in section 2.3) were subjected to discharge followed by charge under identical conditions in 9 M potassium hydroxide solution. The redox processes during charge-discharge have been discussed in our previous work [26].

The discharge-charge profiles of the modified and unmodified EMD electrodes with respect to its voltage were shown in Figure 6. The calculated energy storage performance is based on the mass of EMD for both modified and unmodified electrodes. It is observed that the initial discharge capacity and mid discharge voltage potential of EMD+5C are highest (1.25 V; 280 mAh g^{-1}corresponding to 0.9 e transfer) among all the samples followed by EMD+5C+50F, EMD and EMD+50F. All the cells are found to be rechargeable, although only the modified samples are readily reversible and the extent is found to be high for surfactant and C added sample. The charging profile of unmodified EMD seems to be different from the one modified with F127. Thus, EMD+50F and EMD+5C+50F showed sharp charging behaviour than the EMD and EMD+5C samples suggesting the presence of surfactant aid in faradaic reactions [30].

Figure 7 showed the profile for discharge capacities vs. cycle number, which revealed that with the increase in F127 concentration in the bath from 10 to 25 mg dm^{-3} the initial discharge capacity of the electrodeposited EMD increased, however the discharge capacity attains stability only after about 25^{th} cycle. When the surfactant concentration in the bath was increased to 50 mg dm^{-3}, the material showed good cyclic stability with discharge capacity of about 100 mAh g^{-1} even at the end of 32 cycles in comparison to the blank EMD having discharge capacity of just

35 mAh g^{-1}. However, further increase in the surfactant concentration did not have much impact on discharge capacity and cycleability. Increasing the concentration of the surfactant further to 500 mg dm^{-3} the discharge capacity as well as the cycleability decreased, suggesting 50 mg dm^{-3} would be the suitable critical micelle concentration. At a higher concentration of >50 mg dm^{-3}, the electrode surface may be less accessible to the protons, led to admicelles, affect the adsorption and transfer processes [20].

Figure 8 showed the discharge capacity profile of EMDs deposited from a bath in the absence and presence of C. Increasing the concentration of carbon from 0.5 C to 5 C increases the discharge capacity from 230 to 280 mAh g^{-1}. However the obtained capacity then decreased slowly and attained a discharge capacity of 64 mAh g^{-1} at the end of 32 cycles, reflecting a loss of 78%. Although the presence of carbon in the EMD deposit enhances the conductivity and its initial discharge capacity but the longevity is affected. This may be due to the inhomogeneity of carbon deposition on the EMD surface as patches, in the absence of surfactant, led to an irreversible behaviour. Nevertheless, the achieved performance for the Zn-MnO_2 battery is superior to that of reported earlier [20-28]. Figure 9 showed the comparison study of the discharge capacity vs. cycle numbers of EMDs prepared in the presence of F127, C, C+F127 and the blank EMD (unmodified). EMD modified with F127 showed lower initial discharge capacity (160 mAh g^{-1}) but had better retention in capacity (65%) after 25 cycles, on the other hand carbon modified EMD showed high discharge capacity (280 mAh g^{-1}) but with low capacity retention of only 30%. However EMD+5C+50F showed an intermediate behaviour of EMD+5C and EMD+50F in terms of both discharge capacity and capacity retention. It showed an improved initial discharge capacity of 258 mAh g^{-1} (much higher than EMD+50F), and was able to retain the capacity of 78 mAh g^{-1} even after 32 cycle which is better than EMD+5C. The added

surfactant and carbon changes the porous structure (as evidence through FESEM images in Fig. 5) of the as-prepared electrode and facilitate the charge transfer and hence the observed capacity. To the best of our knowledge, this discharge capacity and the rechargeability of the Zn-MnO_2 battery are considerably higher compared with most of the reported alkaline rechargeable battery technology in the literature [20-28].

Cyclic Voltammetry

To demonstrate the redox (electron transfer) behavior of the as-prepared MnO_2 samples, cyclic voltammetric studies were carried out on the EMDs prepared in the absence and presence of carbon and/or F127. Figures 10 and 11 showed some typical current voltage profiles of the EMD samples prepared in the absence and presence of C and/or F127. The scan was initiated at 0.2 V vs Hg/HgO in the cathodic direction through a reduction maxima (at -0.31V) to -0.6 V causing reduction of the MnO_2 species and then reversing back to the initial potential through an oxidation peak (at 0.08V). The reduction and oxidation maxima are due to the redox species Mn^{+4}/Mn^{+3} for all the scans irrespective of the type and concentrations of the surfactant and carbon used in the bath. Although in all the cases there is no significant change in the shape of the voltammograms, but the additives used (C and F127) affects the peak currents and the peak potentials indicating their presence in the electrolytic bath. It can be seen that in the presence of F127 in the bath the peak currents (both oxidation and reduction) increased at all the concentrations and oxidation potential shifted less negative values and reduction peak current shifted less positive values except at very high concentration of F127 (500 mg dm^{-3}). This indicates that the peak separation minimises for the optimal amount of surfactant indicating the material is well reversible [46 – 47] and the enhanced area under the peak denotes the improved energy storage for 50 and 100 F samples. The increased peak currents indicate better faradaic

behaviour of the EMDs in the presence of F127 [30]. Presence of low concentration (0.5 C) of carbon in Fig. 11 does not have much impact of the electrochemical behaviour, but when its concentration increases to 5C the peak current increases with well-defined behavior, indicating the role of porous nature aids the adsorption/desorption of ions from the aqueous electrolyte. The sharp peak observed for EMD+5C sample indicates fast charge transfer due to highly accessible pore structure suggesting rapid and unhindered diffusion of ions [48] as a result of which the sample showed highest initial discharge capacity than the others. This is in agreement with the galvanostatic charge-discharge results observed in Fig. 9. However the EMD at this high concentration of carbon seems to be unstable showing quick capacity loss with repeated cycles. Introducing the additive F127 with carbon again stabilises the adsorption behaviour of MnO_2 and identified that between 50 and 100 mg dm^{-3} gives better stability and capacitance to EMDs.

Electrochemical Impedance Spectroscopy (EIS) studies

EIS was performed to further investigate the electrochemical behaviour of the EMD in the absence and presence of C and/or F127 respectively associated with charge transfer resistance of the material. Electrochemical impedance spectroscopy was carried out with amplitude of 5 mV over a frequency range of 1 mHz to 100 kHz at open circuit potential. The Nyquist plots displayed in the EIS data (Figs. 12 – 14) are composed of a semicircle in the high frequency region and an inclined line in the low frequency region represent the charge transfer process at electrode/electrolyte interface, and characteristics of diffusion limiting step in electrochemical processes [49]. Combination of electrolytic resistance, intrinsic resistance of the substrate and contact resistance at the active material or interface of current collector (graphite) as a whole give rise to the internal resistance for the material. Figure 12 showed the comparison of the EIS data of the EMD samples in the absence and presence of different concentrations of F127. The solution resistance (R_s) in the high frequency region for the unmodified and modified (50F) is 20

Ω and 5 Ω respectively. The charge transfer resistance (R_{ct}), calculated from the diameter of the semicircle, for the unmodified and modified (50F) is 50 Ω and 4 Ω respectively. The low resistance and low frequency Warburg impedance indicates the material with surfactant has improved electrochemical characteristics. The observed result suggested that the poor performance of EMD with continuous charge discharge cycling (Fig. 7) was due to high impedance value corresponds to high resistance as well as diffusion limitation behaviour of the material. However with increase in F127 concentration in the bath from, 0 to 100 mg dm^{-3} impedance of the material decreased suggesting more conductive behaviour of EMD+50F and EMD+100F, on further increase in F127 concentration in the bath to 500 mg dm^{-3}, EMD+500F showed higher impedance than the earlier concentrations suggesting the fact that tuning of optimum concentration of additive is essential in order to get effective electrochemical activity of modified EMD. Figure 13 showed the EIS plots of EMD samples modified with C. The plots revealed that both EMD+5C and EMD+0.5 C had relatively lower impedance than the EMD deposited from a carbon free bath which implied that conductive carbon present in EMD could increase the electrical conductivity of the modified material in-terms of contact resistance. The increased Rct is a representative of faradaic resistance which is quite high (50 Ω) for unmodified electrode [50]. From the EIS plot shown in Figure 14, EMD+5C+50F showed intermediate behaviour between C and F127 with a distorted semicircle at high frequency region. The highly conducting carbon and surfactant ensure the utilization of the rod-like MnO_2 in terms of both lower charge transfer and low ion diffusion resistance.

Conclusions

In summary, rod-like MnO_2 were electrodeposited via a scalable electrochemical process where both non-ionic surfactant (Pluronic F127) and activated carbon were added in the electrolytic

bath. To achieve improved cycling stability and energy storage in alkaline Zn-MnO_2 battery, synergistic effect of F127 and carbon was investigated to see their role on the physico-electrochemical properties of EMD. From this study it can be concluded that:

- The EMDs produced predominantly consist of γ-MnO_2 and are independent of the presence of additive F127 and/or C in the bath during electrodeposition.
- Nitrogen adsorption-desorption analysis suggested that BET surface area of the EMDs increase with the addition of F127 and/or C to the electrolytic bath.
- Scanning electron micrographs indicated that all the samples show mesoporous characteristics with rod-like network structure; however the size of the crystallites and their orientation varied in the presence of F127 and/or C in the bath.
- In the presence of F127 the EMDs show better capacitive behaviour and cycling ability.
- The optimum concentration of F127 is 50-100 mg dm^{-3} in the absence of carbon, and in the presence of carbon a concentration of 50 mg dm^{-3} is better suited. For EMD + 5C + 50F the obtained initial capacity is 258 mAh g^{-1} and after 30 cycles 78 mAh g^{-1} of the discharge capacity is retained.

Acknowledgements

This research was supported under ARC's Discovery Projects funding scheme (DP1092543). The views expressed herein are those of the authors and are not necessarily those of the Australian Research Council. The authors acknowledge the use of Curtin University's Microscopy and Microanalysis Facility, whose instrumentation has been partially funded by the University, State and Commonwealth Governments.

References

1 L. Li, Z. Wu, S. Yuan and X. -B Zhang, *Energy Environ. Sci*., 2014, **7**, 2101-2122.

2 Z. -L. Wang, D. Xu, J. -J. Xu and X. -B. Zhang, *Chem. Soc. Rev*., 2014, **43**, 7746-7786.

3 A. Urfer, G.A. Lawrance and D.A.J. Swinkels, *J. Appl. Electrochem*. 1997, **27**, 667-672.

4 K.V. Kordesch and M. Dekker, 1974, Batteries. Dekker, New York.

5 K.V. Kordesch and M. Welssenbacher, *J. Power Sources,* 1994*,* **51**, 61-78.

6 E. Machefaux, L.I. Hill and D. Guyomard, *The Electrochem. Soc. 204th Meeting*, Abstract # **365** (2003).

7 W. Jantscher, L. Binder, D.A. Fiedler, R. Andreau and K. Kordesch, *J. Power Sources,* 1999, **79**, 9-18.

8 S. Chou, F. Cheng and J. Chen, *J. Power Sources,* 2006, **162**, 727-734.

9 W. Zhang and Y.C. Chu, *Hydrometallurgy,* 2007, **89**, 137-159.

10 M.M. Sharma, B. Krishnan, S. Zachariah and C.U. Shah, *J. Power Sources,* 1999, **79**, 69-74.

11 http://mesaminerals.com.au/prospects/emd-market-context (Accessed on 05/08/2015).

12 V. Raghuveer and A. Manthiram, *J. Power Sources,* 2006, **159***,* 1468-1473.

13 V. Raghuveer and A. Manthiram, *J. Power Sources,* 2006, **163**, 598-603.

14 M. Minakshi, D.R.G. Mitchell and K. Prince, *Solid State Ionics,* 2008, **179**, 355-361.

15 V. Raghuveer and A. Manthiram, *Electrochem. Commun*. 2005, **7**, 1329-1332.

16 M. Minakshi, and R.G. Mitchell, *Electrochim. Acta,* 2008, **53**, 6323-6327.

17 Q. Wang, J. Pan, Y. Sun and Z. Wang, *J. Power Sources,* 2012, **199**, 355-359.

18 L. Binder, W. Jantscher, F. Hofer and G. Kothleitner, *J. Power Sources,* 1998, **70**, 1-7.

19 H. Tamura, K. Ishizeki, M. Nagayama and R. Furuichi, *J. Electrochem. Soc*. 1994, **141**, 2035-2040.

20 M. Ghaemi, L. Khosravi-Frad and J. Neshati, *J. Power Sources,* 2005, **141**, 340-350.

21 R.K. Ghavami, Z. Rafiei and S.M. Tabatabaei, *J. Power Sources,* 2007, **164**, 934-946.

22 S. Devaraj and N. Munichandraiah, *J. Electrochem. Soc*. 2007, **154**, A901-A909.

23 Suhasini and A.C. Hegde, *J. Electroanal. Chem*. 2012, **676**, 35-39.

24 H. Zhang, Y. Wang, C. Liu and H. Jiang, *J. Alloys Compd*. 2012, **517**, 1-8.

25 H. Zhang., J. Gu, Y. Jiang, J. Zhao, X. Zhang and C. Wang, *J. Solid State Electrochem*. 2014, **18**, 235-247.

26 A. Biswal, B.C. Tripathy, T. Subbaiah, D. Meyrick and M. Minakshi, *J. Solid State Electrochem.* 2013, **17**, 1349-1356.

27 A. Biswal, B.C. Tripathy, T. Subbaiah, D. Meyrick, M. Ionescu and M. Minakshi, *Metall. Mat. Trans. E,* 2014, **1**, 226-238.

28 A. Biswal, B.C. Tripathy, T. Subbaiah, D. Meyrick and M. Minakshi, *J. Electrochem. Soc.* 2015, **162**, A30-A38.

29 P. Yang, D. Zhao, D.I. Margolese, B.F. Chmelka and G.D. Stucky, *Chem. Mater*. 1999, **11**, 2813-2826.

30 P. Yang, D. Zhao, D.I. Margolese, B.F. Chmelka and G.D. Stucky, *Nature,* 1998, **396**, 152-155.

31 P.C.A. Alberius, K.L. Frindell, R.C. Hayward, E.J. Kramer, G.D. Stucky and B.F. Chmelka, *Chem. Mater*. 2002, **14**, 3284-3294.

32 D. Zhao, P.D. Yang, N. Melosh, Y.L. Feng, B.F. Chmelka and G. Stucky, *Adv. Mater*. 1998, **10**, 1380-1385.

33 N.A. Melosh, P. Davidson and B.F. Chmelka, *J. Am. Chem. Soc*. 2000, **122**, 823-829.

34 P. Feng, X. Bu, G.D. Stucky and D.J. Pine, *J. Am. Chem. Soc*. 2000, **122**,, 994-995.

35 P. Feng, X. Bu and D.J. Pine, *Langmuir,* 2000, **16**, 5304-5310.

36 L. Wang, X. Chen, J. Zhan, Y. Chai, C. Yang, L. Xu, W. Zhuang and B. Jing, *J. Phys. Chem. B,* 2005, **109**, 3189-3194.

37 T. Xue, C. L. Xu, D.D Zhao, X. H. Li and H.L. Li, *J. Power Sources,* 2007, **164**, 953-958.

38 J. Veliscek-Carolan, R. Knott and T. Hanley, *J. Phys. Chem*. C, 2015, **119**, 7172-7183.

39 Y. Peng, Z. Chen, J. Wen, Q. Xiao, D. Weng, S. He, H. Geng and Y. Lu, *Nano Res*. 2011, **4**, 216-225.

40 Y. Xu, Y. Zhu and C. Wang, *J. Mater. Chem. A,* 2014, **2**, 9751-9757.

41 S. Sun, C. Matei, G. Raphaël J. Jean-Marc, Le. Meins, A. Cassel, C. Davoisne, C. Masquelier and C. Vix-Guterl, *Microporous and Mesoporous Mater.* 2014, **198**, 175-184.

42 Z. -L. Wang, D. Xu, H. -X. Zhong, J. Wang, F.-L. Meng and X. -B. Zhang, *Sci. Adv.* 2015, **1**, 2-9.

43 M. Selvam, S. R. Srither, K. Saminathan and V. Rajendran, *Ionics,* 2015, **21**, 791-799.

44 Z. Wu, X.-L. Huang, Z.-L. Wang, J.-J. Xu, H. -G. Wang and X. -B. Zhang, *Sci. Rep*, 2014, **4** , 1-8.

45 Z. -L. Wang, D. Xu, H. -G. Wang, Z. Wu and X. -B. Zhang, *ACS Nano*, 2013, **7**, 2422–2430.

46 N. Li, C. J. Patrissi, G. Che and C. R. Martin, *J. Electrochem. Soc.* 2000, **147**, 2044-2049.

47 M. Minakshi and D. Meyrick, *Electrochim. Acta*, 2013, **101**, 66 – 70.

48 E. Bertel and N. Memmel, *Appl. Phys. A,* 1996, **63**, 523-531.

49 R. K. Sharma and L. Zhai, *Electrochim. Acta,* 2009, **54**, 7148-7155.

50 Y. Qiao, C. L. Li, S. J. Bao and Q. L. Bao, *J. Power Sources,* 2007, **170**, 79 – 84.

Table 1 Effect of F127 and C on the current Efficiency (CE), Energy Consumption (EC) of the EMD samples

Type of EMD	**Current Efficiency (CE) %**	**Energy Consumption (EC) kWh.kg^{-1}**
EMD	98.5	1.697
EMD+10F	100	1.580
EMD+25F	100	1.501
EMD+50F	100	1.579
EMD+100F	100	1.630
EMD+500F	99	1.692
EMD+C0.5	85	1.732
EMD+C5	80	1.750
EMD+C5+50F	88	1.720

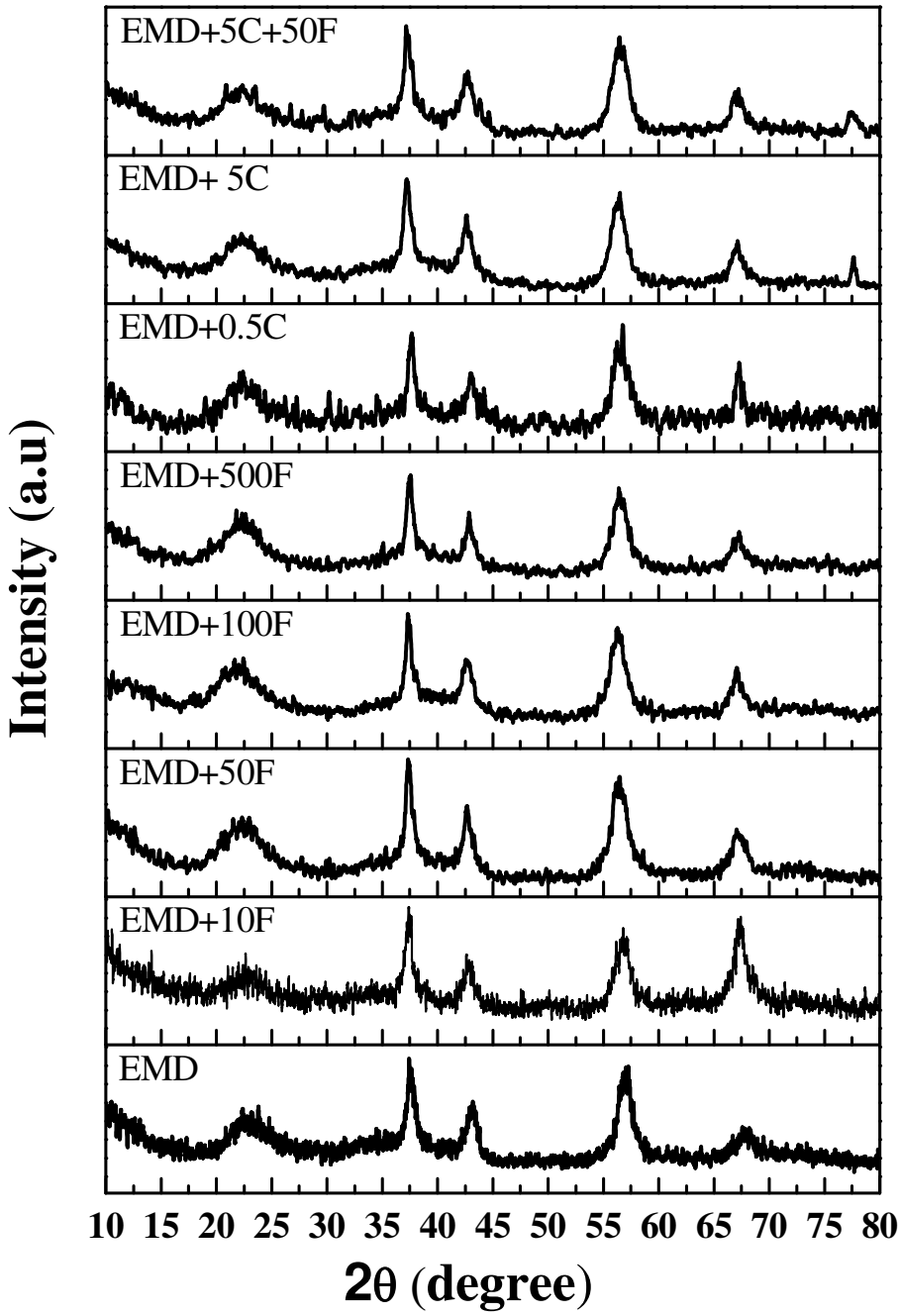

Figure 1 X-ray diffraction pattern of EMD samples in absence and presence of different concentrations of surfactant (F127), activated carbon (C) and both.

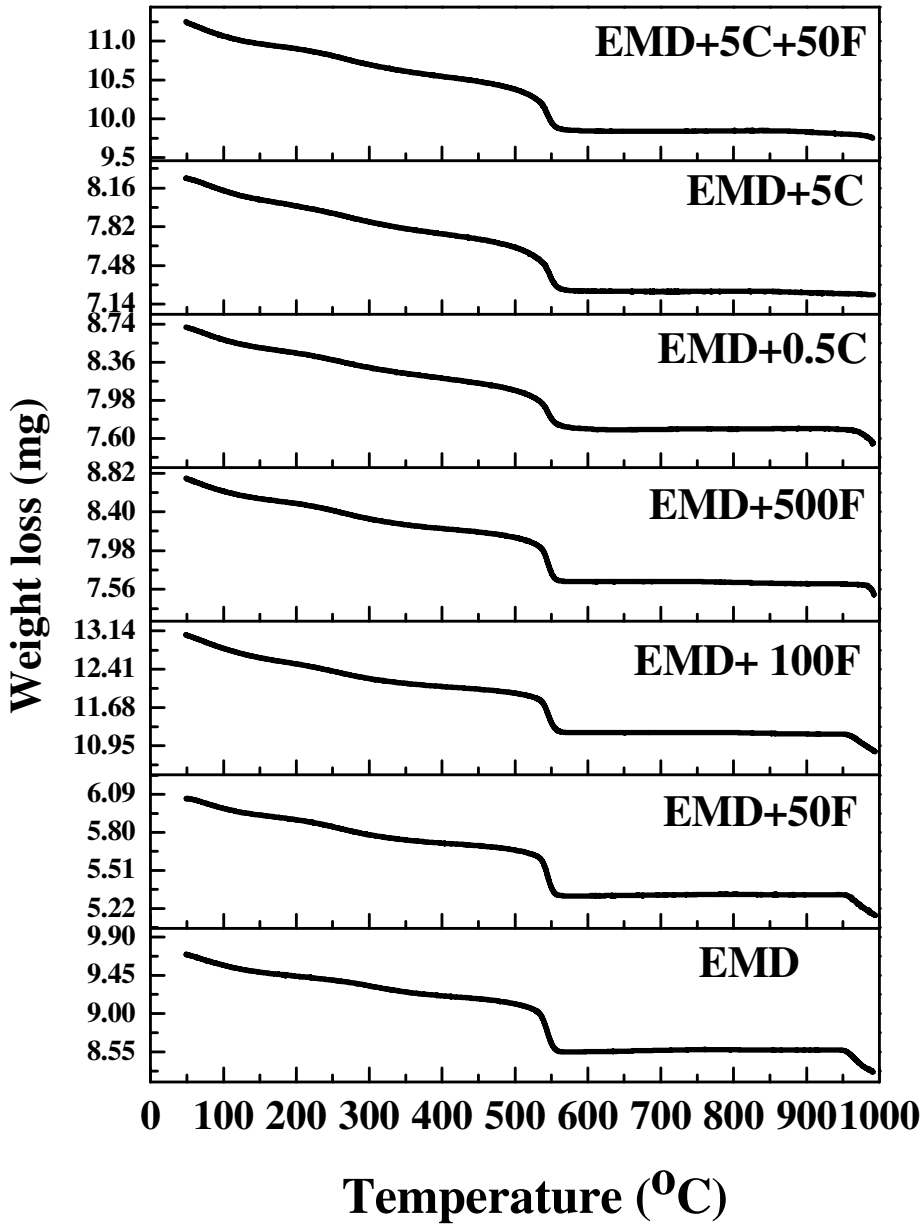

Figure 2 Thermo gravimetric (TG) plots of EMD samples in the absence and presence of different concentrations of F127, C and both.

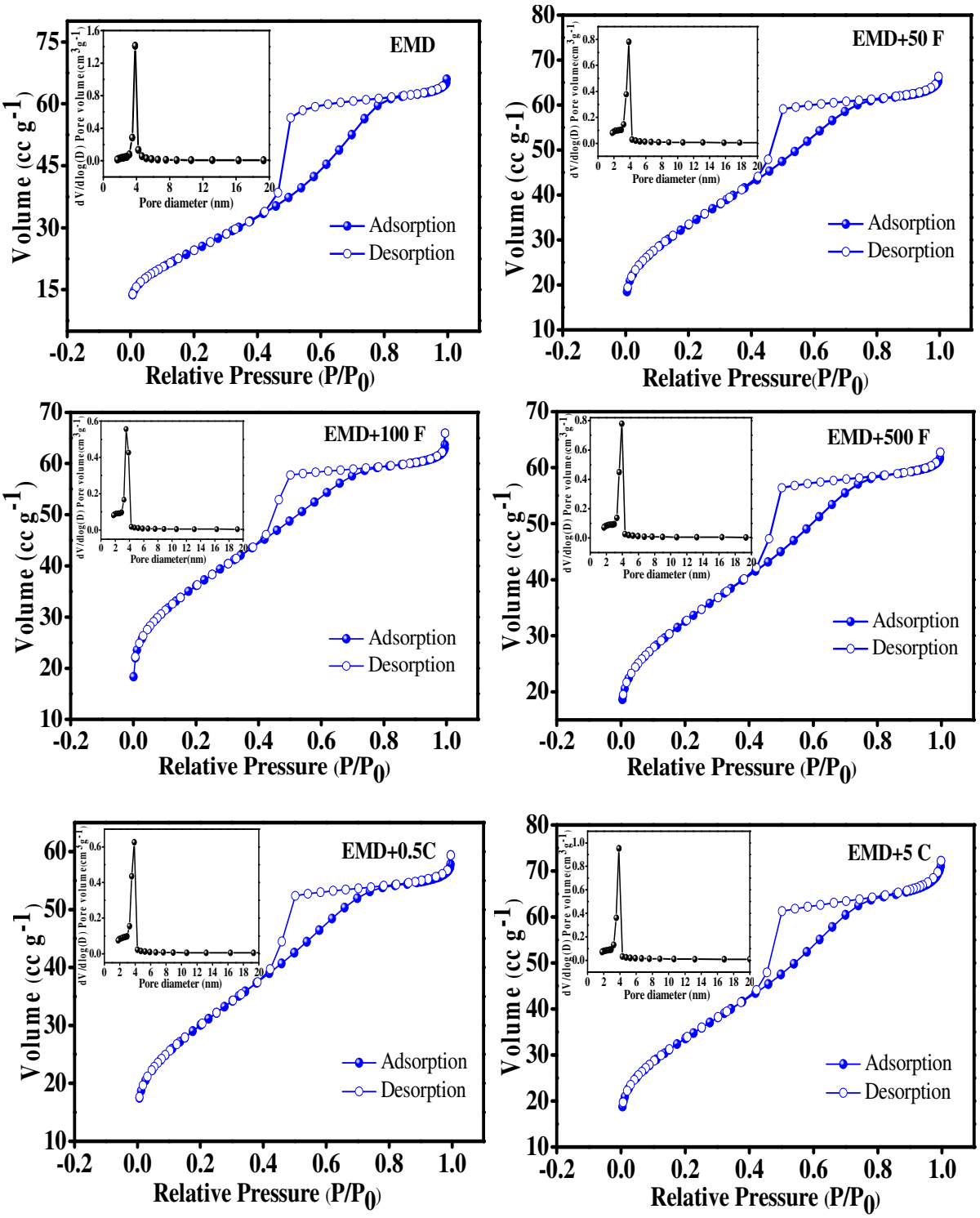

Figure 3 Nitrogen adsorption and desorption isotherm of EMD samples absence and presence of different concentrations of F127 and C. (Inset- Pore size distribution curve)

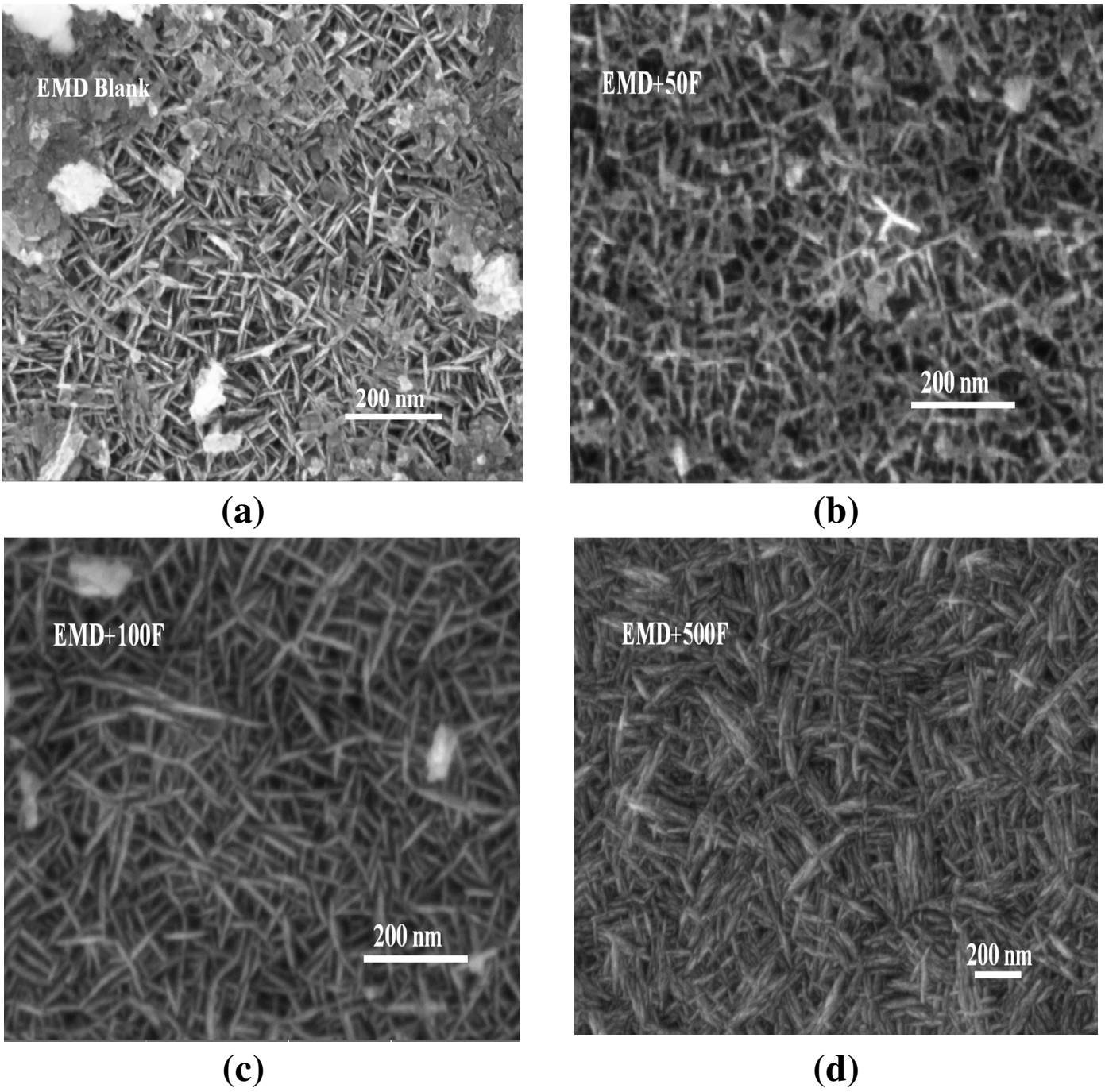

Figure 4 Field emission SEM (FESEM) images of as-prepared EMD samples deposited from a bath (a) additive free, (b) 50 mg dm^{-3} F127, (c) 100 mg dm^{-3} F127, and (d) 500 mg dm^{-3} F127

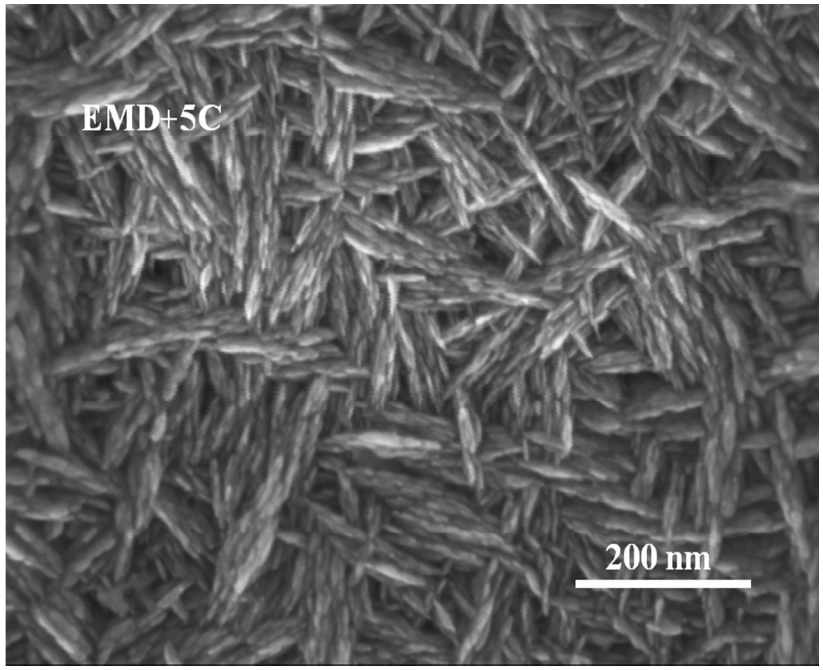

(a)

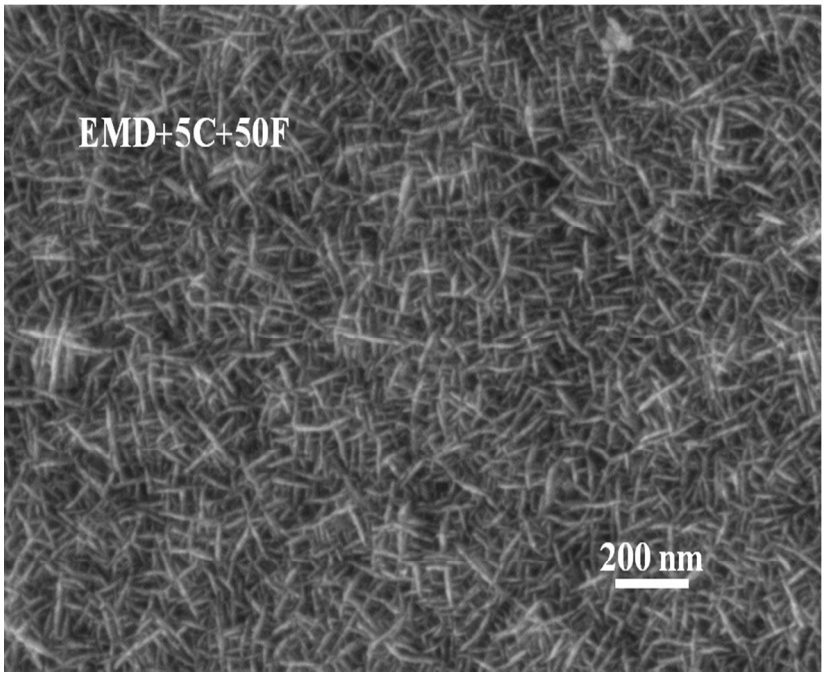

(b)

Figure 5 FESEM images of as-prepared EMD samples showing rod-like morphology, deposited from a bath containing (a) 5 g dm^{-3} of C, and (b) containing 5 g dm^{-3} of C + 50 mg dm^{-3} of F127

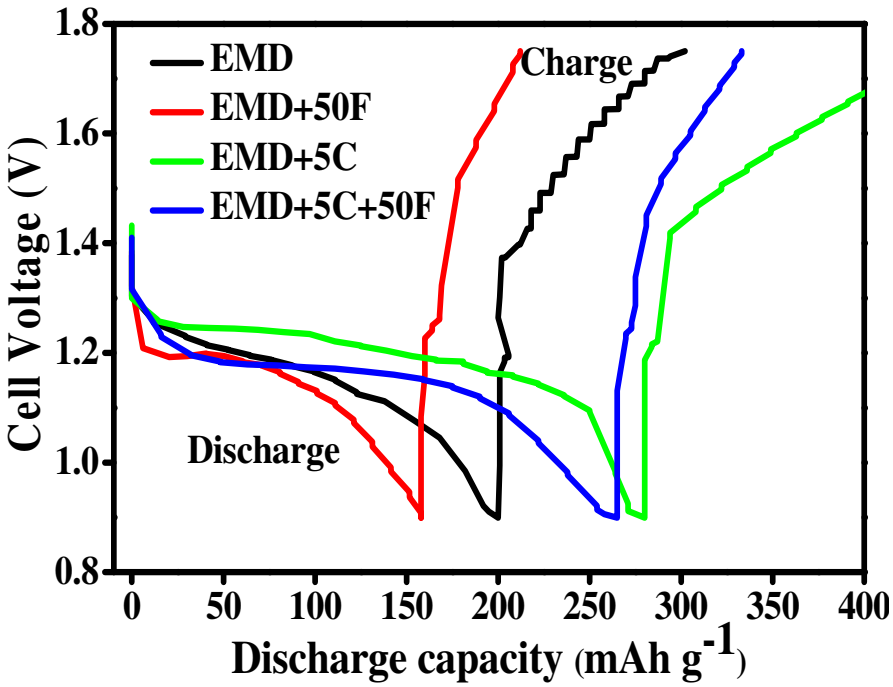

Figure 6 The first discharge-charge profile of Zn/EMD cell (modified and unmodified) using 9M KOH.

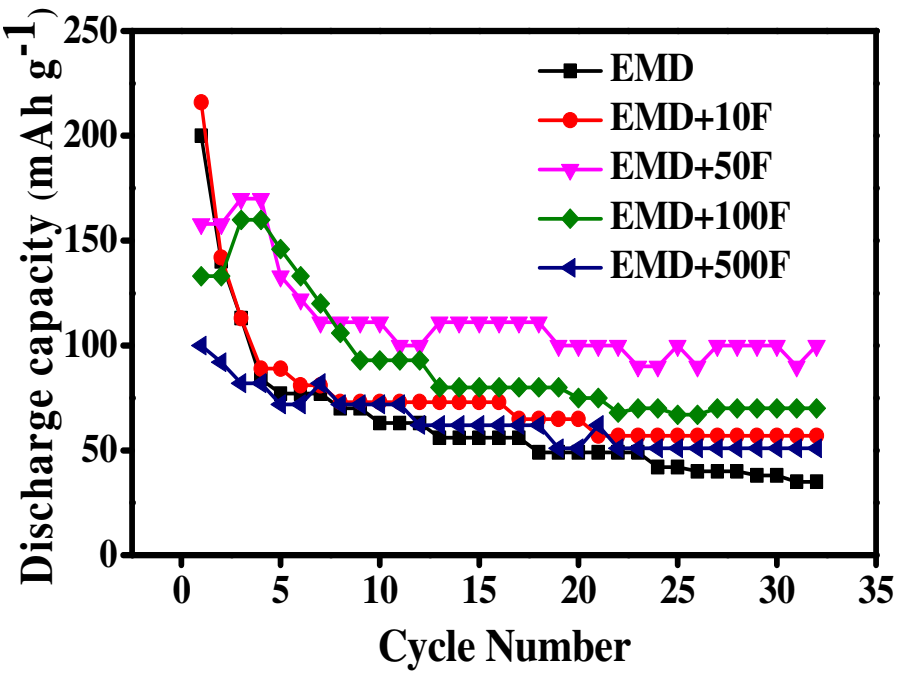

Figure 7 Discharge capacity versus cycling behaviour of EMD at different concentrations of F127.

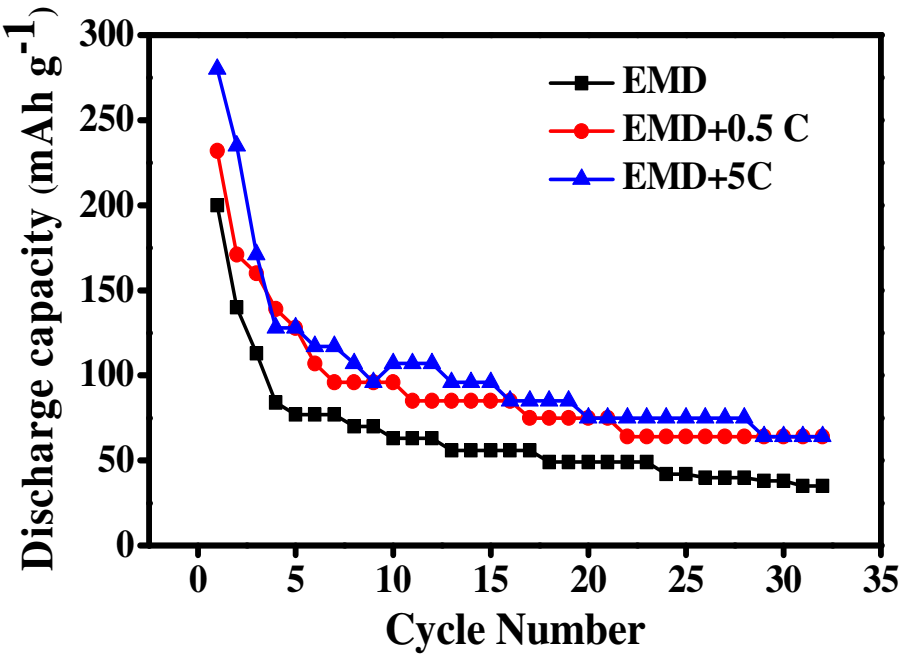

Figure 8 Discharge capacity versus cycling behaviour of EMD at different concentrations of C.

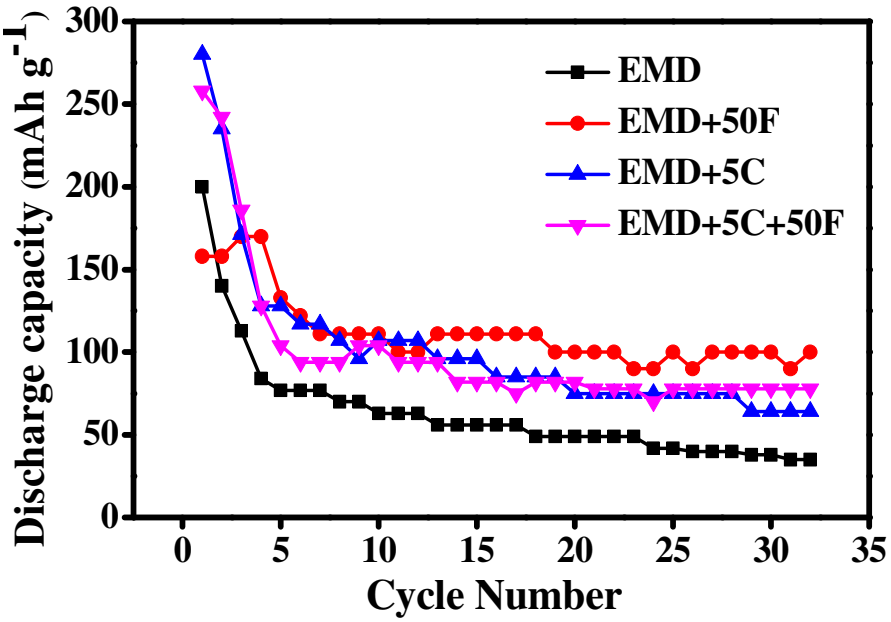

Figure 9 Discharge capacity versus cycling behaviour of unmodified and modified EMD samples with 50F, 5C and in the presence of both additives (50F + 5C).

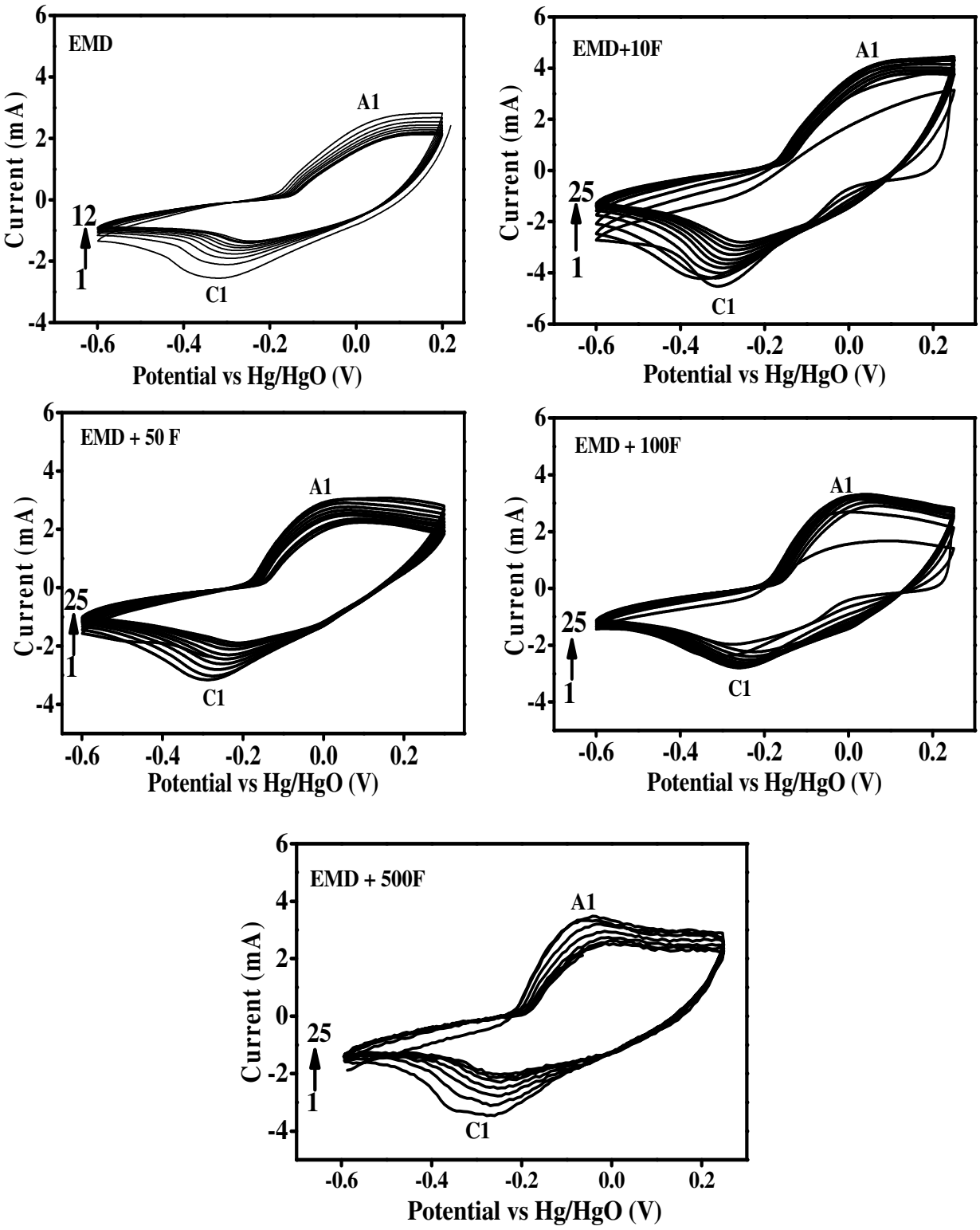

Figure 10 Cyclic voltammetry plots of EMD samples in the absence and presence of different concentrations of F127 at a scan rate of 0.2 mVs^{-1}. The term "C" and "A" denotes reduction (cathodic) and oxidation (anodic) peaks respectively. Cycle numbers are indicated in the figure.

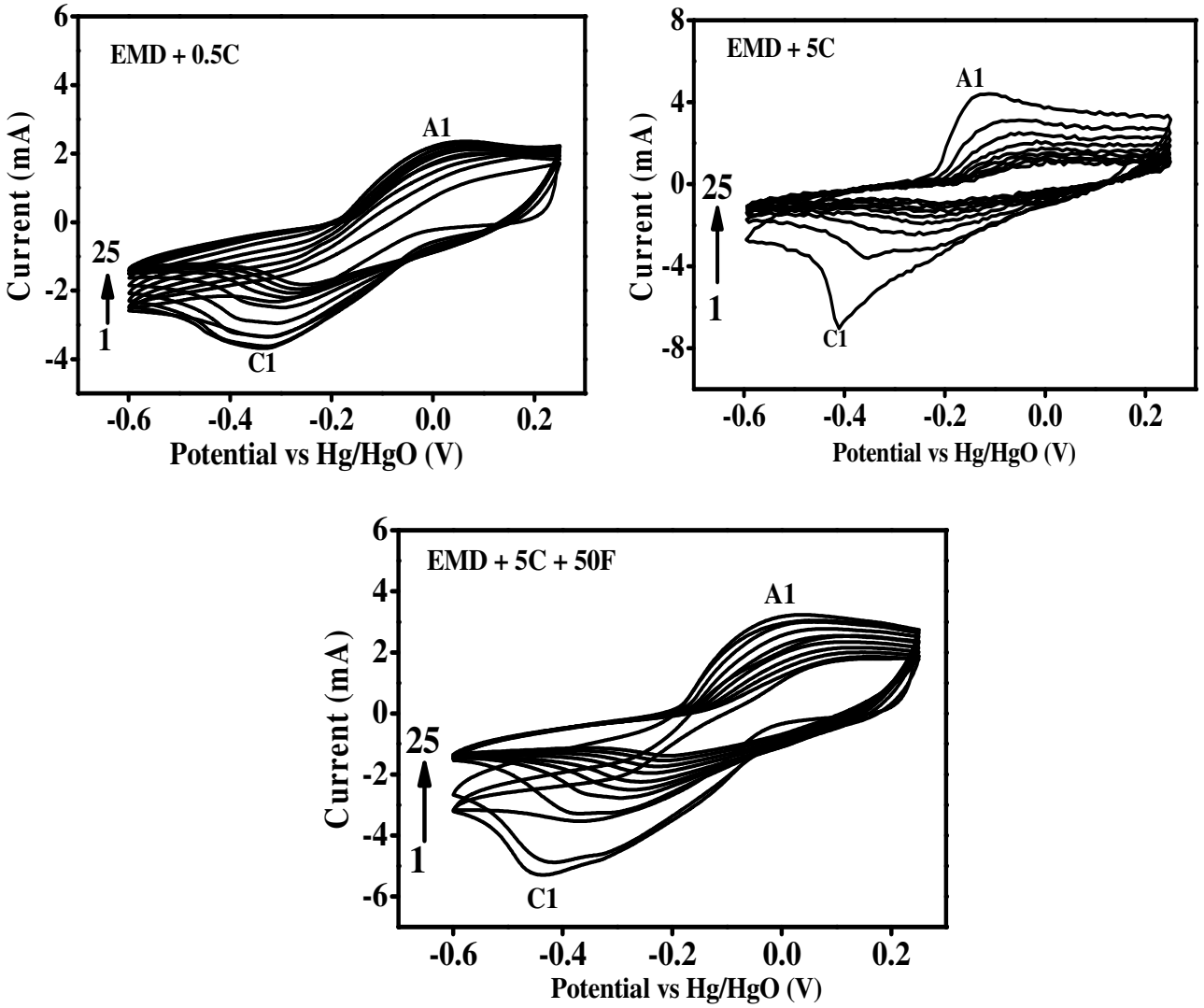

Figure 11 Cyclic voltammetry plots of EMD samples in the absence and presence of different concentrations of C and both additives (50F + 5C) at a scan rate of 0.2 mV s^{-1}. The term "C" and "A" denotes reduction (cathodic) and oxidation (anodic) peaks respectively. Cycle numbers are indicated in the figure.

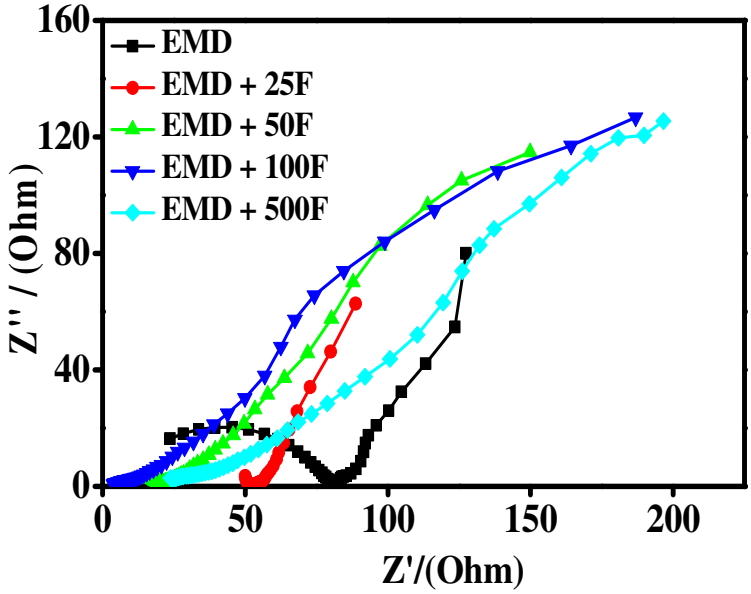

Figure 12 EIS plots of EMD samples in the absence and presence of different concentrations of F127.

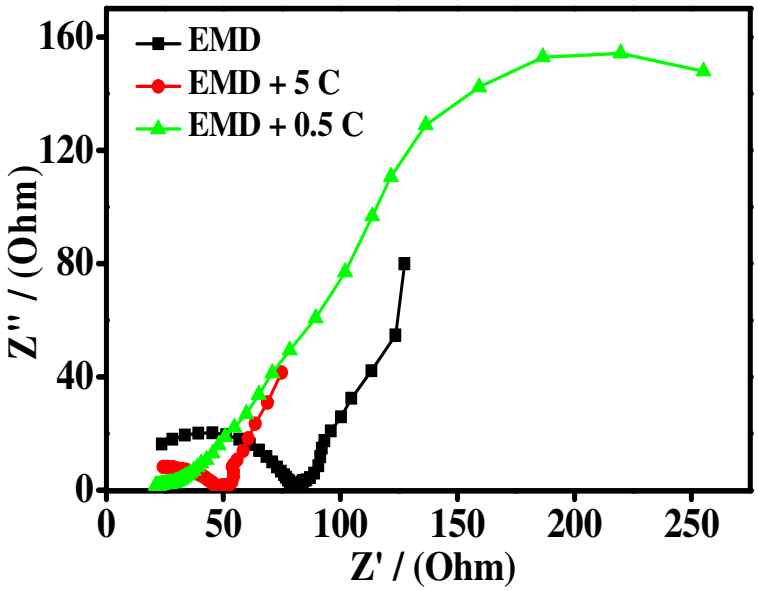

Figure 13 EIS plots of EMD samples in the absence and presence of different concentrations of C.

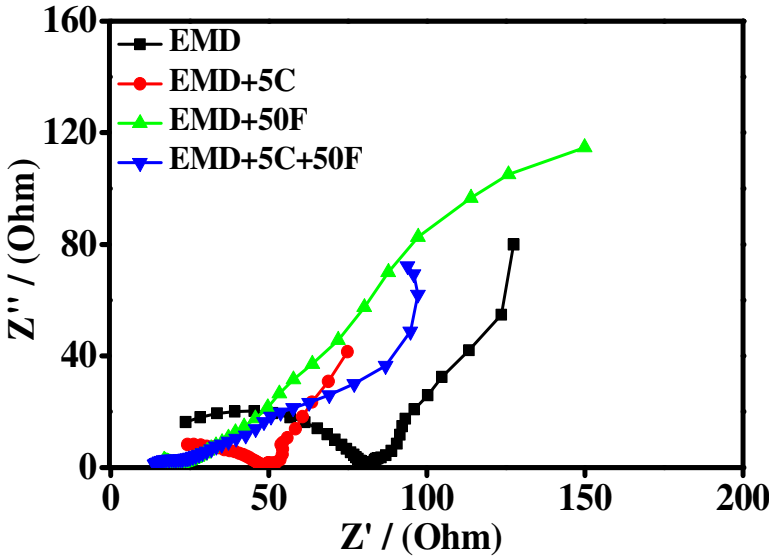

Figure 14 EIS plots of unmodified and modified EMD samples with 50F, 5C and in the presence of both additives (50F + 5C).

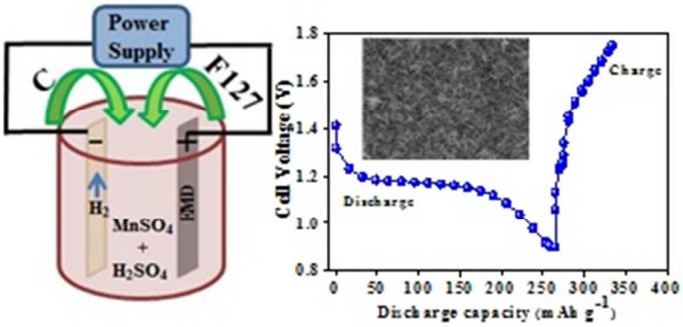

Synergistic effect of F127 and carbon on EMD with superior performance for use in alkaline rechargeable battery is reported.